Research Square

Preprints are preliminary reports that have not undergone peer review.
They should not be considered conclusive, used to inform clinical practice,
or referenced by the media as validated information.

Identification of ovarian non-coding RNAs as biomarkers for post-emergence age estimation in the forensically important Sarcophaga peregrina (Diptera: Sarcophagidae)

Jiayi Wang
Central South University
Lele Tian
Central South University
Xinrong Ren
Central South University
Hai Wu
Central South University
Pei Liu
Central South University
Chengxin Ye
Central South University
Yadong Guo
Central South University
Yanjie Shang
shangyj@csu.edu.cn
Central South University

Research Article

Keywords: Forensic entomology, Sarcophaga peregrina, Postmortem interval, Circular RNAs, Long non-coding RNAs, ovarian transcriptome

Posted Date: November 24th, 2026

DOI: https://doi.org/10.21203/rs.3.rs-11565348/v1

License: This work is licensed under a Creative Commons Attribution 4.0 International License.
Read Full License

Additional Declarations: No competing interests reported.

Identification of ovarian non-coding RNAs as biomarkers for post-emergence age estimation in the forensically important *Sarcophaga peregrina* (Diptera: Sarcophagidae)

Author: Jiayi Wang [a], Lele Tian [a], Xinrong Ren [a], Hai Wu [a], Pei Liu [a], Chengxin Ye [a], Yadong Guo [a], Yanjie Shang [a,*]

[a] Department of Forensic Science, Xiangya School of Basic Medical Sciences, Central South University, Changsha 410013, Hunan, China

***Corresponding Author:**Yanjie Shang
Xiangya School of Basic Medical Sciences, Central South University, Changsha 410013, Hunan, China;
E-mail: shangyj@csu.edu.cn

Funding

This work was supported by the National Natural Science Foundation of China (grant number 82402196), the Natural Science Foundation of Hunan Province (grant number 2024JJ6546), Graduate Innovation Project of Central South University (grant number 2026ZZTS0145).

Identification of ovarian non-coding RNAs as biomarkers for post-emergence age estimation in the forensically important *Sarcophaga peregrina* (Diptera: Sarcophagidae)

Abstract: Accurate estimation of the age of necrophagous flies is important for postmortem interval (PMI) assessment in forensic entomology. However, molecular approaches for estimating the post-emergence age of adult flies remain limited. This study investigated temporal changes in ovarian long non-coding RNAs (lncRNAs) and circular RNAs (circRNAs) in female *Sarcophaga peregrina* and evaluated their potential as molecular markers for adult age estimation. Whole-transcriptome sequencing of ovaries collected at 1, 3, 5, 7, and 9 days after emergence identified pronounced age-related changes in lncRNA and circRNA expression. Time-series screening followed by real-time quantitative PCR validation using independent biological samples identified eight non-coding RNAs significantly associated with post-emergence age. Regression analysis showed that the combination of circRNA_1081 and TCONS_00010107 provided the best overall prediction, with mean absolute errors of 0.481 and 0.534 days under leave-one-out and leave-one-age-group-out cross-validation, respectively. These findings demonstrate that ovarian lncRNAs and circRNAs contain temporal information associated with post-emergence development and may provide molecular markers for age estimation of adult *S. peregrina*, extending the potential application of molecular age assessment beyond immature developmental stages.

Keywords: Forensic entomology · *Sarcophaga peregrina* · Postmortem interval · Circular RNAs · Long non-coding RNAs · ovarian transcriptome

1.Introduction:

Accurate estimation of the postmortem interval (PMI) is an important component of forensic practice, as it helps define the time frame of death, reconstruct case events, and provide temporal evidence for criminal investigations and judicial decision-making[1]. As the postmortem period increases, conventional PMI estimation methods based on postmortem changes and physicochemical indicators become increasingly limited[2]. Forensic entomology provides important evidence for PMI estimation, particularly the minimum postmortem interval (PMI_{min}), by analyzing the species, developmental stages, and growth patterns of insects associated with decomposing remains[3]. Accurate determination of the developmental age of necrophagous insects is therefore a key step in estimating PMI_{min} from entomological evidence[4].

Current forensic entomological age-estimation studies have focused primarily on immature stages, including eggs, larvae, and pupae. Larval age can be estimated using indicators such as body length, body weight, and developmental stage[5], whereas the relatively limited external morphological changes during the pupal stage have prompted the development of additional approaches based on histomorphology[6], gene expression[7], cuticular hydrocarbons, and spectroscopic analysis[8]. In contrast, post-emergence age estimation in adult flies has received comparatively less attention[9]. However, at some death scenes, particularly in indoor or relatively enclosed environments, adults that complete development and emerge from remains may persist for a period of time[10]. Their post-emergence age may therefore extend the temporal information obtainable from entomological evidence. Previous studies have explored adult age estimation using ovarian development[11], ocular pteridine content[10], wing damage, and cuticular hydrocarbons[12], and have shown that some of these indicators change predictably with time after emergence. Nevertheless, these approaches can be influenced by temperature, nutrition, reproductive status, and individual variation, and their temporal resolution and objectivity remain to be improved.

With advances in molecular biology, RNAs exhibiting time-dependent expression patterns have increasingly been applied to insect age estimation. Tarone et al. were among the first to show that the transcript levels of several genes changed predictably over time during blow fly egg development, indicating that gene expression can provide developmental timing information

beyond conventional morphological indicators[13]. Subsequently, Tarone and Foran incorporated developmentally regulated gene expression into larval and pupal age-estimation models and evaluated their performance using blind samples[14]. Boehme et al. identified age-associated gene expression patterns in Calliphora vicina pupae and subsequently assessed their predictive value in three blind studies[15]. In *Sarcophaga peregrina*, several mRNAs showing regular expression changes during pupal development have also been identified, and their potential for pupal age estimation has been validated by real-time quantitative PCR(qRT-PCR)[16]. These studies demonstrate that continuous changes in RNA expression can reflect insect developmental progression and provide an important basis for establishing objective molecular markers of insect age.

In addition to protein-coding mRNAs, non-coding RNAs have attracted increasing attention for their roles in insect growth, development, and reproductive regulation.Long non-coding RNAs (lncRNAs) participate in transcriptional and post-transcriptional regulation[17]. Functional studies have demonstrated roles for specific lncRNAs in insect development and oogenesis, while pathway analyses suggest potential associations with metabolic processes[18, 19]. Circular RNAs (circRNAs) are characterized by covalently closed structures and exhibit a degree of tissue and developmental stage specificity[20]. Previous studies have identified specific lncRNAs and circRNAs whose expression varies with ovarian development and vitellogenesis in insects. Functional studies have also demonstrated roles for selected transcripts in reproductive regulation, suggesting that their expression profiles may provide information about reproductive physiological state[21, 22]. In recent years, non-coding RNAs have also been explored for age estimation in forensic entomology. Wu et al. identified circRNAs showing regular temporal changes during the pupal stage of *S. peregrina* and established a pupal age estimation model using qRT-PCR and regression analysis, further indicating that non-coding RNAs can also carry developmental time-related information[23].

The early post-emergence period in female insects is accompanied by rapid maturation of the reproductive system. As oogenesis and vitellogenesis progress, the ovaries undergo pronounced morphological changes together with broad alterations in hormonal regulation, metabolism, and gene transcription[24]. The ovary may therefore serve as a sensitive tissue for detecting time-related molecular changes associated with post-emergence reproductive maturation[25].

Ovarian morphological indicators have traditionally been used to estimate adult female fly age, indicating that ovarian development can provide age-related information. However, gene expression-based age-estimation studies in forensic entomology have largely focused on immature stages, whereas post-emergence ovarian transcriptional dynamics in necrophagous flies remain insufficiently characterized. In particular, the temporal expression patterns of ovarian lncRNAs and circRNAs after emergence in *S. peregrina*, and their potential utility for adult age estimation, remain underexplored.

Accordingly, this study focused on the ovaries of adult female *S. peregrina*. Ovarian samples were collected at 1, 3, 5, 7, and 9 days after emergence, and whole-transcriptome sequencing was performed to characterize post-emergence transcriptional changes, with particular emphasis on the differential expression and temporal patterns of lncRNAs and circRNAs. Candidate non-coding RNAs showing stable age-related changes were then screened and validated by qRT-PCR using independent biological samples. The potential of individual and combined non-coding RNA markers for post-emergence adult age estimation was further evaluated. This study aimed to identify stable molecular markers of adult age and to provide an experimental basis for the objective estimation of post-emergence age in necrophagous flies and its further application in forensic entomology.

2.Materials and methods

2.1. Experimental colony rearing and ovarian sample collection

In July 2020, adult *S. peregrina* were collected in Changsha, Hunan Province, China, and an experimental colony was established after morphological identification. The colony was maintained for three generations in a controlled-environment chamber before use in subsequent experiments. Rearing conditions were 25±0.5℃, 75±2% relative humidity, and a 12 h:12 h light-dark cycle. Adults were continuously supplied with water and a 1:1 (w/w) mixture of soy milk powder and granulated sugar, and fresh pig lung was provided to induce larviposition. Larvae deposited within 2 h were collected, transferred to clean rearing containers, and provided with sufficient fresh pig lung until pupation. Pupae formed within the same batch were selected and maintained under the same conditions until adult emergence. When approximately 50% of the pupae had emerged, this time point was defined as day 1 of adulthood (D1), and the remaining unemerged pupae were removed. Female adults were collected on D1, D3, D5, D7, and D9. After

sex determination based on terminal abdominal reproductive structures, females were dissected under a stereomicroscope and both ovaries were isolated. Three independent biological replicates were prepared for each age group, with each replicate consisting of pooled bilateral ovaries from 50 females. The collected ovarian samples were immediately frozen in liquid nitrogen and stored at −80℃ until RNA extraction.

2.2.RNA extraction and sequencing

Total RNA was extracted from ovarian samples collected on D1, D3, D5, D7, and D9, with three independent biological replicates per age group and 15 samples in total. RNA was extracted using the mirVana™ miRNA Isolation Kit (Ambion) according to the manufacturer's instructions. RNA concentration and purity were measured using a NanoDrop 2000 spectrophotometer, and RNA integrity was assessed using an Agilent 2100 Bioanalyzer. Samples with an RNA integrity number (RIN) ≥ 7 were used for subsequent library preparation. Ribosomal RNA was depleted using the TruSeq Stranded Total RNA with Ribo-Zero Gold kit, and strand-specific whole-transcriptome libraries were constructed. Following rRNA depletion, RNA was fragmented and first-strand cDNA was synthesized using random hexamer primers. Second-strand cDNA synthesis was then performed with dUTP incorporation to preserve strand specificity. Library construction was completed through end repair, A-tailing, adapter ligation, fragment selection, and PCR amplification. The resulting libraries were quality-checked using an Agilent 2100 Bioanalyzer and subsequently subjected to paired-end sequencing on an Illumina platform.

2.3.Transcriptome data processing and RNA identification

Raw sequencing data were subjected to quality control to obtain clean reads, which were subsequently used for RNA identification and expression quantification. For mRNAs, clean reads were aligned to the *S. peregrina* reference genome[26] using HISAT2[27], and transcripts were assembled with StringTie[28]. Read counts mapped to protein-coding gene regions were quantified using HTSeq-count v0.9.1 in reverse-stranded mode[29]. mRNA expression abundance was expressed as fragments per kilobase of transcript per million mapped reads (FPKM). For lncRNAs, transcripts longer than 200 bp and containing at least two exons were retained, followed by coding potential assessment using CPC2[30], CNCI[31], PLEK[32], and Pfam[33]. lncRNA expression was quantified using Bowtie2 v2.2.9[34] and eXpress v1.5.1[35]. Expression abundance was expressed as transcripts per million (TPM), and estimated counts were used for

differential expression analysis. For circRNAs, clean reads were aligned to the reference genome using BWA[36], and circRNAs were identified with CIRI2[37] based on back-splice junction reads and associated splice signals. circRNA expression levels were quantified according to back-splice junction reads and expressed as reads per billion mapped reads (RPB).

2.4.Differential expression and temporal analysis

Differential expression was analyzed between adjacent age groups (D3 vs D1, D5 vs D3, D7 vs D5, and D9 vs D7). Differentially expressed lncRNAs were identified from raw count data using DESeq2 v1.22.2[38]. Library sizes were normalized using size factors, and differential expression was assessed using a negative binomial model, with P values adjusted by the Benjamini–Hochberg method. Differentially expressed circRNAs were analyzed using DEGseq v1.36.1[39], with expression levels represented by RPB values calculated from back-splice junction reads. For both RNA types, q-value < 0.05 and $|\log_2 FC| \geqslant 1$ were considered significant. Before temporal trend analysis, RNAs with fewer than 10 total raw counts across the 15 samples or detected in fewer than three samples were excluded. Post-emergence age was coded as 1, 3, 5, 7, and 9 days, and Spearman correlations with age were calculated using TPM values for lncRNAs and RPB values for circRNAs. Multiple testing was corrected separately for each RNA type using the Benjamini–Hochberg method. RNAs with $|\rho| \geqslant 0.80$ and FDR < 0.05 were considered strongly age-associated, and only those showing a strictly monotonic change in mean expression across D1-D9 were retained. lncRNAs were additionally required to be differentially expressed in at least two adjacent-age comparisons, whereas circRNAs were required to meet this criterion in at least one comparison. A lower threshold was applied to circRNAs because their quantification relied on back-splice junction reads, which generally yielded lower counts. Expression stability was then evaluated using the coefficient of variation (CV) among the three biological replicates at each age, and RNAs with a median CV > 1.0 across the five age groups were excluded. The remaining RNAs were prioritized according to the number of significant adjacent-age comparisons, absolute Spearman correlation coefficient, within-age stability, expression abundance, and detection completeness. Functional annotation and non-redundancy among candidates were further considered when selecting RNAs for qRT-PCR validation using independent samples. To investigate the biological functions associated with differentially expressed lncRNAs and circRNAs, Gene Ontology (GO) and Kyoto Encyclopedia of Genes and

Genomes (KEGG) enrichment analyses were performed on their associated protein-coding genes. For lncRNAs, cis-associated protein-coding genes with isBest = 1 were extracted from FEELnc predictions[40]. For circRNAs, host protein-coding genes were obtained from circRNA annotations, and circRNAs without annotated host genes were excluded. After removing duplicate genes within each comparison, GO and KEGG enrichment analyses were performed using a hypergeometric test followed by Benjamini–Hochberg correction, with FDR < 0.05 considered significant. GO analysis focused on biological process terms. For each adjacent-age comparison, the five significant GO biological process terms and KEGG pathways with the lowest FDR values were visualized; all significant terms were shown when fewer than five were identified, whereas no terms were displayed when none reached statistical significance.

2.5.Quantitative real-time (qRT)-PCR analysis

To validate the candidate non-coding RNAs identified by RNA-seq, qRT-PCR was performed using an independent set of ovarian samples collected on D1, D3, D5, D7, and D9, with three biological replicates per age group. Total RNA was extracted using the SteadyPure Universal RNA Extraction Kit (Accurate Biotechnology (Hunan) Co., Ltd., China). Primers for the candidate lncRNAs, circRNAs, and Actin were designed using Primer 5.0 (Premier Biosoft, Palo Alto, CA, USA), and the primer sequences used in subsequent analyses are listed in Tables 1 and 2. Actin was selected as the reference gene based on its previous use in qRT-PCR analyses of developmental expression in *S. peregrina*[23]. qRT-PCR was performed using the SYBR® Green Premix Pro Taq HS qPCR Kit (ROX Plus; Accurate Biotechnology) on an ABI 7500 Real-Time PCR System. Each sample was analyzed in triplicate technical wells, with no-template controls included, and amplification specificity was assessed by melting-curve analysis. Relative expression levels were calculated using the $2^{-\Delta\Delta}$Ct method, with the D1 group used as the calibrator. For each biological sample, the mean Ct value of the three technical replicates was used to calculate ΔCt. Spearman rank correlation analysis was performed to assess the association between ΔCt values and post-emergence age, with multiple testing corrected using the Benjamini–Hochberg method. Candidate RNAs for subsequent adult age prediction modeling were selected based on correlation strength, trends in mean ΔCt across age groups, biological replicate stability, data completeness, and qRT-PCR amplification quality.

Table 1 Primers used for qRT-PCR analysis of the selected lncRNA DEGs

RNA type	RNA name	Primer	Primer sequence (5′–3′)
Reference gene	Actin	Forward	AAGAACAAGGTGAAGAGGGAC
		Reverse	TCGTCTTCATCGCGGAATATG
the DEGs	TCONS_00049193 (lnc193)	Forward	ACATGCTGGTTGTCCTGTTCTAA
		Reverse	GGTCTCACCAATTCTTGTCTACG
	TCONS_00010107 (lnc107)	Forward	CGCTTATGATGACAACGATCCTA
		Reverse	AGGTGGTGAATAAACTCTTGGCT
	TCONS_00036632 (lnc632)	Forward	ACCGCATACATTCGCTATCATCA
		Reverse	GGGCAAGGCATGGTGTTT
	TCONS_00016628 (lnc628)	Forward	CATTGTTGGTCTACTGCGGC
		Reverse	AATCGGTTCAGGGGTTGAGG

Table 2 Primers used for qRT-PCR analysis of the selected circRNA DEGs

RNA type	RNA name	Primer	Primer sequence (5′–3′)
Reference gene	Actin	Forward	AAGAACAAGGTGAAGAGGGAC
		Reverse	TCGTCTTCATCGCGGAATATG
the DEGs	circRNA_1081 (circ369)	Forward	TGATGATGAGACGGATGAAATCG
		Reverse	TCATTACAATTCGGTACGCCATTA
	circRNA_4838 (circ009)	Forward	CTTCATTGTTCTGGTGGCTGTTT
		Reverse	ACATTTCTCTGGCTAAGGAGCAG
	circRNA_2726 (circ654)	Forward	GGCTATATCTGTCCTATGGCTGT
		Reverse	TATCAGACTTGTTGCGACTGGAA
	circRNA_0243 (circ643)	Forward	GCTGCAACATCGACAACAACAAT
		Reverse	TATGATTCGCTTTACGAGGTGGA

2.6.Age prediction model development and validation

For each biological sample, the mean Ct value of three technical replicates was used to calculate ΔCt (ΔCt = Ct_target − Ct_Actin). A total of 15 independent biological samples from D1, D3, D5, D7, and D9 were included, with three samples per age group. Based on the qRT-PCR validation results, four lncRNAs and four circRNAs were selected for model development. Post-emergence age was used as the dependent variable and RNA ΔCt values as predictors. Ordinary least-squares regression was used to construct eight single-marker linear models, and all pairwise combinations of the eight RNAs were further evaluated, resulting in 28 two-marker models. Internal predictive performance was assessed using leave-one-out cross-validation (LOOCV) and leave-one-group-out cross-validation (LOGO-CV), with age group used as the grouping factor. The arithmetic mean of the MAEs obtained from the two cross-validation strategies was used as the overall error metric, and the combination with the lowest overall error was selected as the final model. Model performance was evaluated using mean absolute error (MAE), root mean square error (RMSE), and the cross-validated coefficient of determination (Q^2). The final regression equation was refitted using all 15 samples.

3.Results

3.1.Characterization of the ovarian transcriptome

Ovarian samples from adult female *S. peregrina* collected at 1, 3, 5, 7, and 9 days after

emergence (D1, D3, D5, D7, and D9) were subjected to whole-transcriptome sequencing. Three biological replicates were included for each age group, yielding a total of 15 sequencing libraries. Sequencing generated 187.3 Gb of clean data, with 10.65 – 14.02 Gb obtained per sample. The proportion of Q30 bases ranged from 96.50% to 97.05%, and the mean GC content was 40.18% (Table S1). After quality control, reads were aligned to the *S. peregrina* reference genome, with overall mapping rates of 86.74% – 91.43% and uniquely mapped read rates of 77.72% – 87.28% across samples (Table S2). These results indicate that the transcriptomic data were of sufficient quality for subsequent identification and expression analysis of mRNAs, lncRNAs, and circRNAs.

3.2. Identification of ovarian non-coding RNAs in *S. peregrina*

Whole-transcriptome analysis identified 14,700 mRNAs, 18,890 lncRNAs, and 6,756 circRNAs. The number of lncRNAs detected was generally comparable across samples (Fig. 1A). lncRNAs ranged from 201 to 10,569 nt in length, with a mean length of approximately 507 nt, and most were distributed within the shorter length range (Fig. 1B). Based on their genomic position and orientation relative to protein-coding genes, 18,230 lncRNAs were classified as genic exonic, genic intronic, intergenic upstream, intergenic downstream, and other positional categories, whereas 660 lncRNAs could not be assigned to a defined positional category (Fig. 1C). Exon structure analysis showed that most lncRNAs contained two or three exons, indicating an overall tendency toward relatively simple exon structures (Fig. 1D).

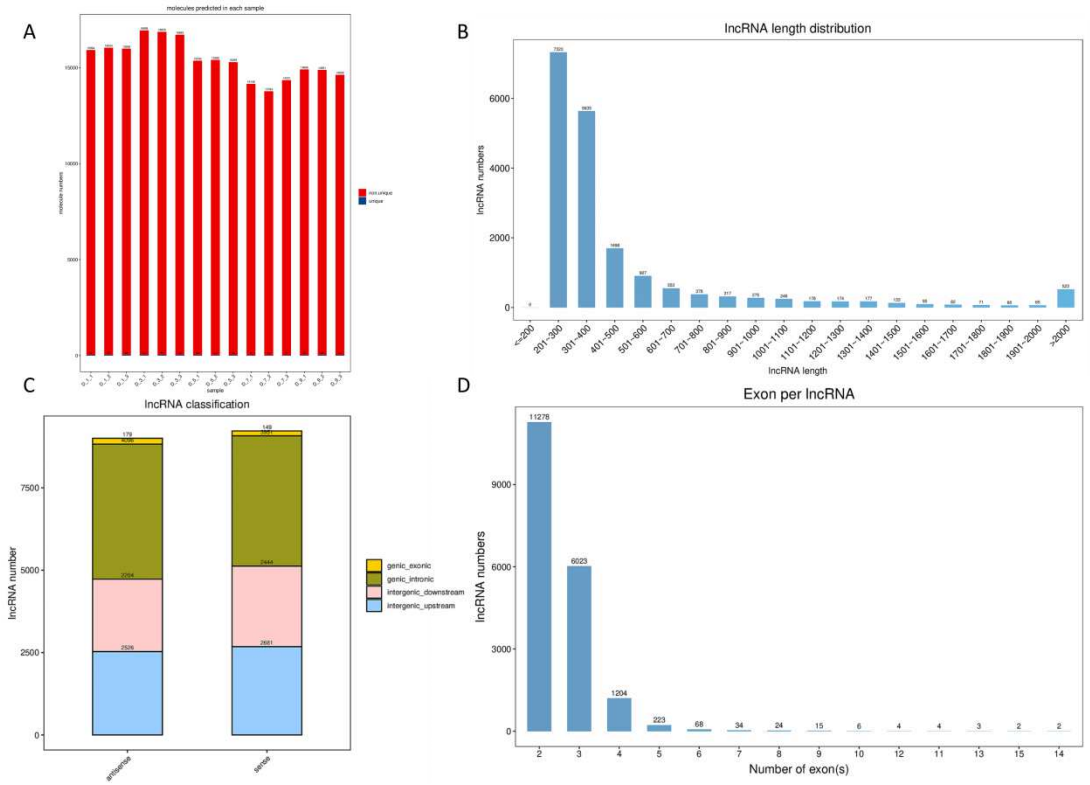

Fig. 1. Characteristics of ovarian lncRNAs identified in adult female *S. peregrina*. (A) Numbers of lncRNAs detected in each sample. Blue indicates sample-specific lncRNAs detected only in the corresponding sample, whereas red indicates non-specific lncRNAs detected in more than one sample. (B) Length distribution of the identified lncRNAs. (C) Classification of lncRNAs according to their genomic positions and orientations relative to protein-coding genes. Of the 18,890 identified lncRNAs, 18,230 were assigned to the displayed categories, whereas the remaining 660 lacked an assigned category and are not shown. (D) Exon number distribution of the identified lncRNAs.

The number of circRNAs detected varied to some extent among samples (Fig. 2A). circRNAs ranged from 112 to 98,386 nt in length, with a mean length of approximately 3,438 nt, and most were shorter than 2,000 nt (Fig. 2B). Based on genomic origin, sense-overlapping circRNAs were the most abundant, with 3,718 identified (55%), followed by intergenic circRNAs (1,390; 21%), antisense circRNAs (907; 13%), exonic circRNAs (601; 9%), and intronic circRNAs (140; 2%) (Fig. 2C). Exon structure analysis showed that circRNAs were mainly composed of one to three exons, with single-exon circRNAs being the most common (Fig. 2D).

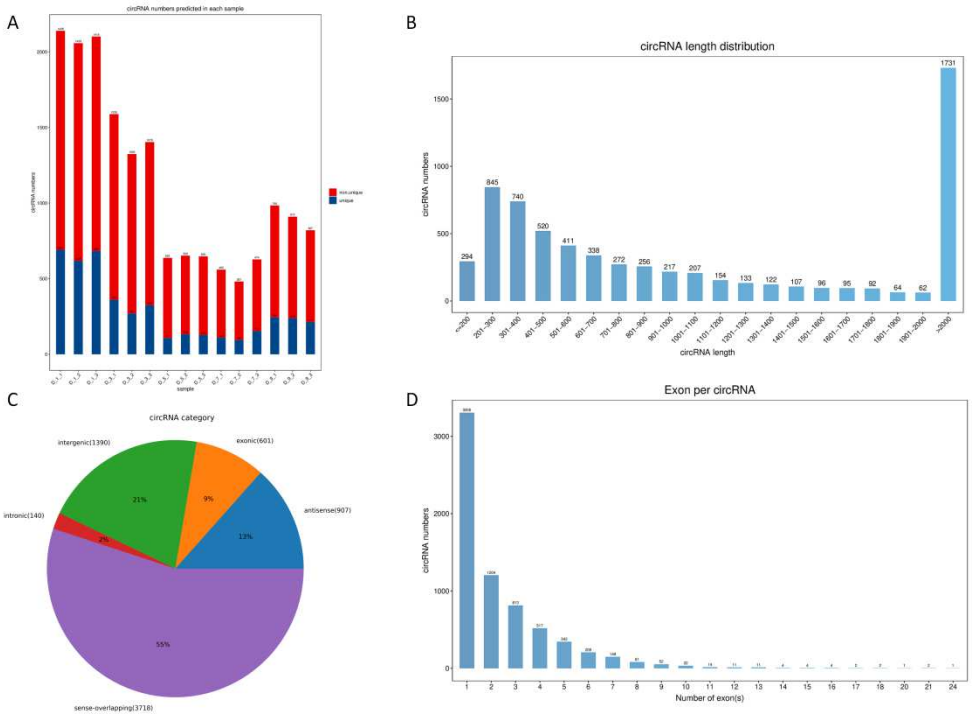

Fig. 2. Characteristics of ovarian circRNAs identified in adult female *S. peregrina*. (A) Numbers of circRNAs detected in each sample; blue and red indicate unique and non-unique circRNAs, respectively. (B) Length distribution of circRNAs. (C) Genomic classification of circRNAs, with counts and percentages shown for each category. (D) Exon number distribution of circRNAs.

Principal component analysis showed that the three biological replicates within each age group generally clustered together, whereas samples from different age groups showed a degree of separation. The first two principal components explained 54.88% and 31.67% of the total variance in mRNA expression data (Fig. 3A), 45.63% and 24.79% in lncRNA expression data (Fig. 3B), and 29.40% and 24.29% in circRNA expression data (Fig. 3C), respectively. These results indicate good consistency among biological replicates and age-related differences in the overall expression patterns of all three RNA types.

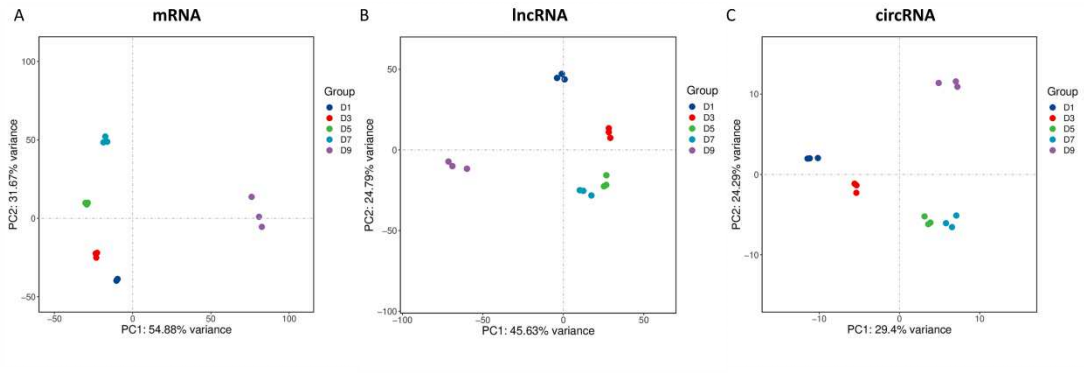

Fig. 3. Principal component analysis of ovarian RNA expression profiles in *S. peregrina* at different post-emergence ages. Principal component analysis of (A) mRNA, (B) lncRNA, and (C) circRNA expression profiles. Each point represents one biological replicate, and colors distinguish the five age groups (D1, D3, D5, D7, and D9; n = 3 per group). Percentages on the axes indicate the variance explained by the first two principal components.

3.3.Differential expression of ovarian lncRNAs and circRNAs in *S. peregrina* during the post-emergence stage

Using q-value < 0.05 and $|\log_2 FC| \geqslant 1$ as the significance thresholds, differential expression of lncRNAs and circRNAs was analyzed between adjacent age groups. In the D3 vs D1, D5 vs D3, D7 vs D5, and D9 vs D7 comparisons, 4,597, 1,144, 320, and 3,412 differentially expressed lncRNAs were identified, respectively, including 1,442, 582, 248, and 2,256 upregulated lncRNAs and 3,155, 562, 72, and 1,156 downregulated lncRNAs (Fig. 4A). The corresponding comparisons identified 876, 685, 259, and 547 differentially expressed circRNAs, including 272, 111, 96, and 400 upregulated circRNAs and 604, 574, 163, and 147 downregulated circRNAs, respectively (Fig. 4B). Complete differential expression results are provided in Tables S3-S4. Comparison of the four adjacent-age contrasts showed that 36 lncRNAs and 15 circRNAs were differentially expressed in all four comparisons. In addition, 1,878, 278, 60, and 915 lncRNAs, together with 482, 223, 47, and 221 circRNAs, were uniquely differentially expressed in D3 vs D1, D5 vs D3, D7 vs D5, and D9 vs D7, respectively (Fig. 4C, D). For both non-coding RNA types, the number of differentially expressed transcripts was lowest in D7 vs D5 and

increased again in D9 vs D7, indicating clear age-stage-dependent changes in ovarian non-coding RNA expression in *S. peregrina*.

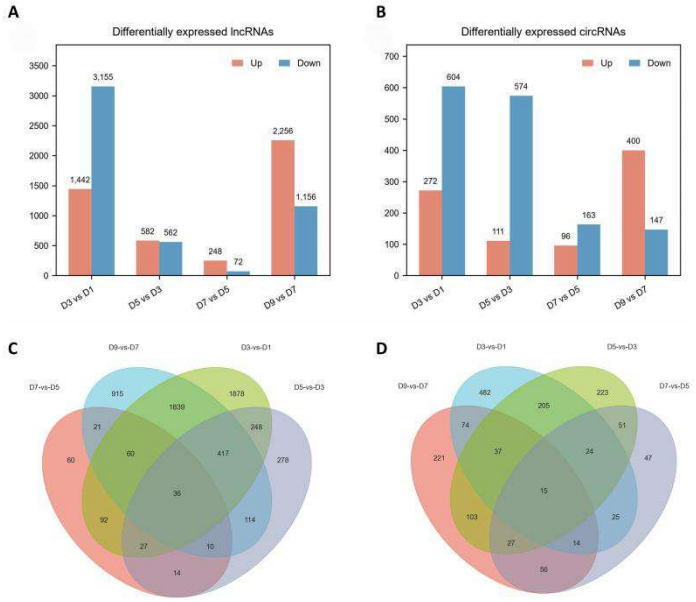

Fig. 4. Differential expression of ovarian lncRNAs and circRNAs between adjacent post-emergence ages in *S. peregrina*. Numbers of differentially expressed (A) lncRNAs and (B) circRNAs in the D3 vs D1, D5 vs D3, D7 vs D5, and D9 vs D7 comparisons. Red and blue bars indicate upregulation and downregulation, respectively, in the later age group relative to the earlier group. Venn diagrams show shared and comparison-specific differentially expressed (C) lncRNAs and (D) circRNAs.

3.4.GO and KEGG enrichment analysis of DE ncRNA-associated genes

To investigate the potential biological functions associated with differentially expressed non-coding RNAs, GO and KEGG analyses were performed on the cis-associated genes of differentially expressed lncRNAs and the host genes of differentially expressed circRNAs. The cis-associated genes of differentially expressed lncRNAs were mainly related to transcriptional regulation, development, and cellular signaling. In D3 vs D1, the enriched terms were primarily associated with transcriptional regulation, cell migration, and morphogenesis, together with the MAPK signaling pathway - fly, axon regeneration, and relaxin signaling pathway. D5 vs D3 was mainly associated with macroautophagy and protein localization-related processes, whereas D7 vs D5 was characterized primarily by the hormone-mediated signaling pathway. In D9 vs D7, terms related to transcriptional regulation and morphogenesis reappeared. No significant KEGG pathways were detected in D5 vs D3 or D7 vs D5 (Fig. S1A, B). The host genes of differentially

expressed circRNAs were mainly associated with cytoskeletal organization, cell junctions, and signal transduction. Actin filament organization was significantly enriched in three consecutive comparisons, including D3 vs D1, D5 vs D3, and D7 vs D5. Other stage-specific processes included regulation of small GTPase-mediated signaling, cell–cell junction organization, egg chorion assembly, protein phosphorylation, and tissue regeneration. KEGG analysis mainly identified the cGMP–PKG, Rap1, ErbB, and Hippo signaling pathways, as well as adherens junction. No significant KEGG pathways were detected in D7 vs D5 (Fig. S1C, D).

Overall, the cis-associated genes of lncRNAs were more strongly associated with transcriptional regulation and developmental processes, whereas circRNA host genes showed more prominent associations with cytoskeletal organization and cell junctions, indicating distinct functional characteristics of the two classes of non-coding RNA-associated genes across post-emergence ovarian developmental stages. Complete GO and KEGG enrichment results for lncRNA cis-associated genes across the four adjacent-age comparisons are provided in Tables S5 and S6, respectively, and those for circRNA host genes are provided in Tables S7 and S8.

3.5.Identification of age-associated non-coding RNAs in *S. peregrina* ovaries

After expression filtering, 17,468 lncRNAs and 1,442 circRNAs were retained for temporal correlation analysis. Among them, 3,706 lncRNAs and 198 circRNAs showed strong correlations with post-emergence age ($|\rho| \geqslant 0.80$, FDR < 0.05). Of these age-associated RNAs, 325 lncRNAs and 44 circRNAs exhibited strictly monotonic increases or decreases in mean expression across D1, D3, D5, D7, and D9. After integration with the adjacent-age differential expression results, 121 lncRNAs and 29 circRNAs were retained. lncRNAs were required to be differentially expressed in at least two adjacent-age comparisons, whereas circRNAs were required to meet this criterion in at least one comparison. Expression stability was then assessed using the coefficient of variation (CV) among the three biological replicates at each age. RNAs with a median CV > 1.0 across the five age groups were excluded, resulting in a candidate pool of 117 lncRNAs and 27 circRNAs. These candidates were further prioritized according to the absolute Spearman correlation coefficient, number of significant adjacent-age comparisons, replicate stability, expression abundance, and detection completeness. Functional annotation and non-redundancy among candidates were also considered, and representative RNAs were selected for qRT-PCR validation using independent samples. Detailed information on the selected candidates is provided

in Table S9.

3.6.Quantitative real-time PCR (qRT-PCR) validation and post-emergence age estimation

Based on the temporal trend analysis, selected lncRNAs and circRNAs were validated by qRT-PCR using ovarian samples independent of those used for RNA-seq. The relative expression levels of TCONS_00049193, TCONS_00010107, circRNA_1081, circRNA_4838, circRNA_2726, and circRNA_0243 decreased continuously from D1 to D9. TCONS_00036632 and TCONS_00016628 showed slight fluctuations between some adjacent age groups but exhibited an overall decreasing trend (Fig. 5). Spearman correlation analysis based on ΔCt values showed that all eight non-coding RNAs were significantly positively correlated with post-emergence age (FDR < 0.05), consistent with their expression trends.

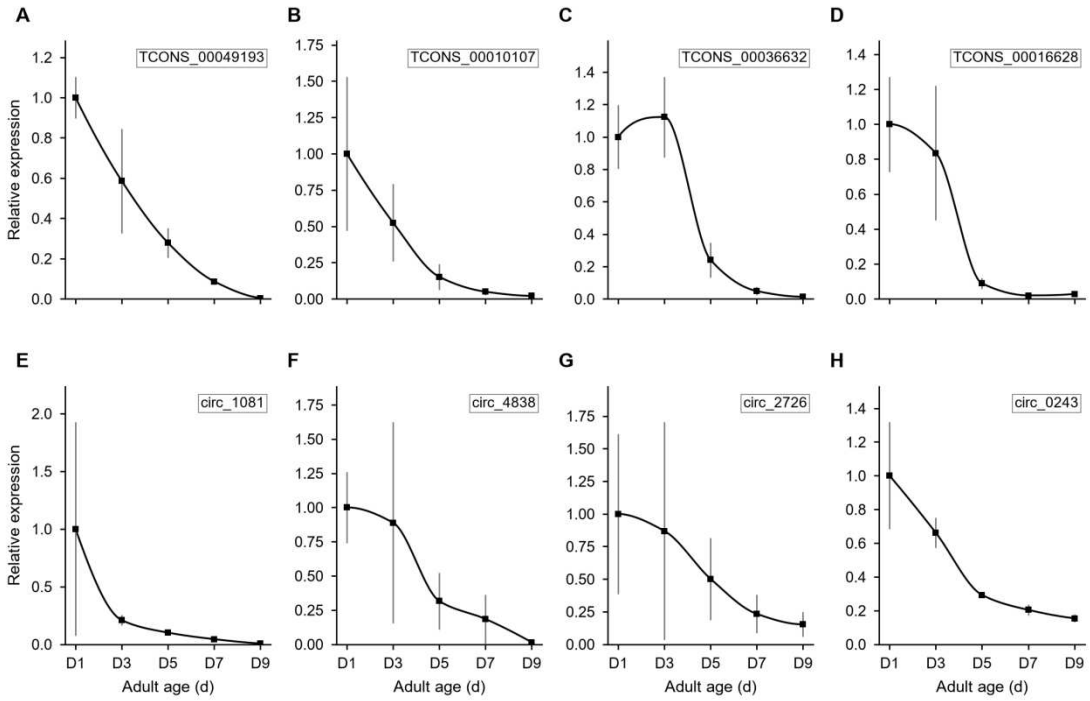

Fig. 5. Relative expression profiles of candidate ovarian lncRNAs and circRNAs during early adulthood in *S. peregrina*. qRT-PCR analysis of (A) TCONS_00049193, (B) TCONS_00010107, (C) TCONS_00036632, (D) TCONS_00016628, (E) circRNA_1081, (F) circRNA_4838, (G) circRNA_2726, and (H) circRNA_0243 at D1, D3, D5, D7, and D9.

Single-marker linear regression models were then constructed and evaluated using leave-one-out cross-validation (LOOCV). The eight models yielded MAEs ranging from 0.767 to 1.740 d. Among them, circRNA_0243, circRNA_1081, TCONS_00010107, and

TCONS_00036632 showed MAEs of 0.767, 0.784, 0.833, and 0.838 d, respectively. The regression equations and performance metrics for all single-marker models are provided in Table S10, and the regression results are shown in Fig. 6.

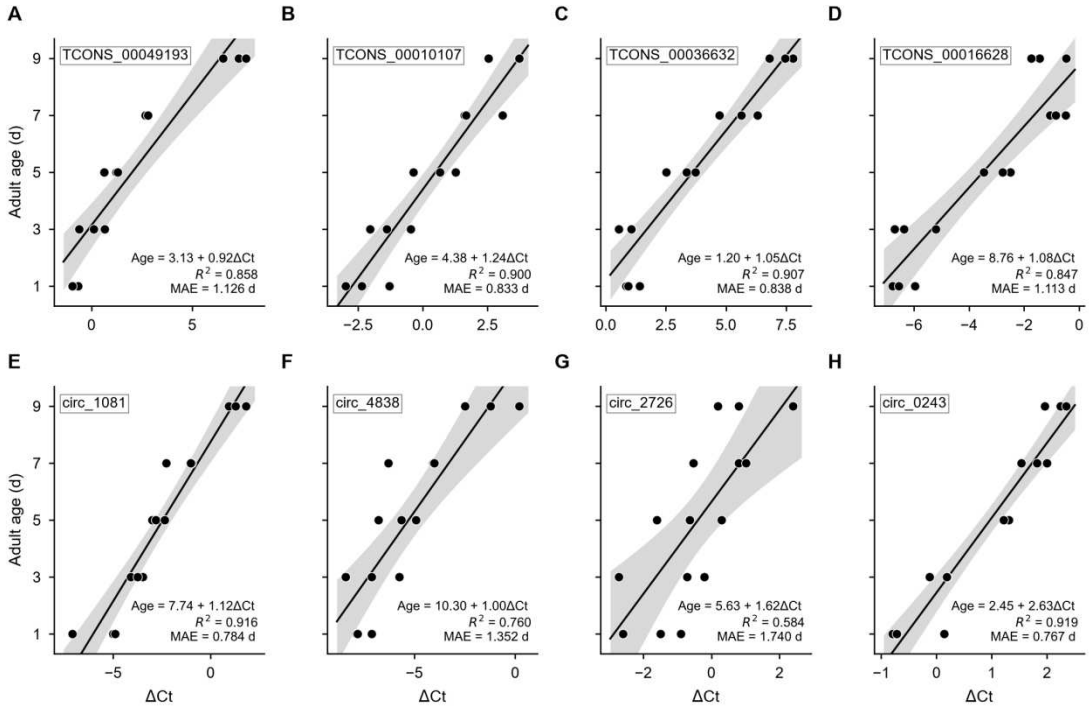

Fig. 6. Single-marker regression models for post-emergence age estimation in adult female *S. peregrina*. Linear relationships between adult age and ovarian Δ Ct values of (A) TCONS_00049193, (B) TCONS_00010107, (C) TCONS_00036632, (D) TCONS_00016628, (E) circRNA_1081, (F) circRNA_4838, (G) circRNA_2726, and (H) circRNA_0243. Each point represents one independent biological sample (n = 15). Solid lines represent ordinary least-squares regression fits, and gray shaded areas indicate 95% confidence intervals. Each panel shows the regression equation, the coefficient of determination calculated from the complete dataset (R^2), and the mean absolute error obtained by leave-one-out cross-validation (MAE).

All 28 pairwise combinations of the eight candidate RNAs were subsequently evaluated using LOOCV and leave-one-group-out cross-validation (LOGO-CV). The combination of circRNA_1081 and TCONS_00010107 achieved MAEs of 0.481 d in LOOCV and 0.534 d in LOGO-CV, with an average MAE of 0.508 d, the lowest among all combinations. This pair was therefore selected as the final two-marker model (Table S11). The regression equation fitted using all 15 samples was:

$$y = 6.2453 + 0.6338\,\Delta Ct(\text{circRNA_1081}) + 0.6176\,\Delta Ct(\text{TCONS_00010107})$$

where y represents the predicted post-emergence adult age (d). The model yielded an MAE, RMSE, and Q^2 of 0.481 d, 0.613 d, and 0.953, respectively, in LOOCV, and 0.534 d, 0.644 d, and 0.948, respectively, in LOGO-CV (Table S12; Fig. 7).

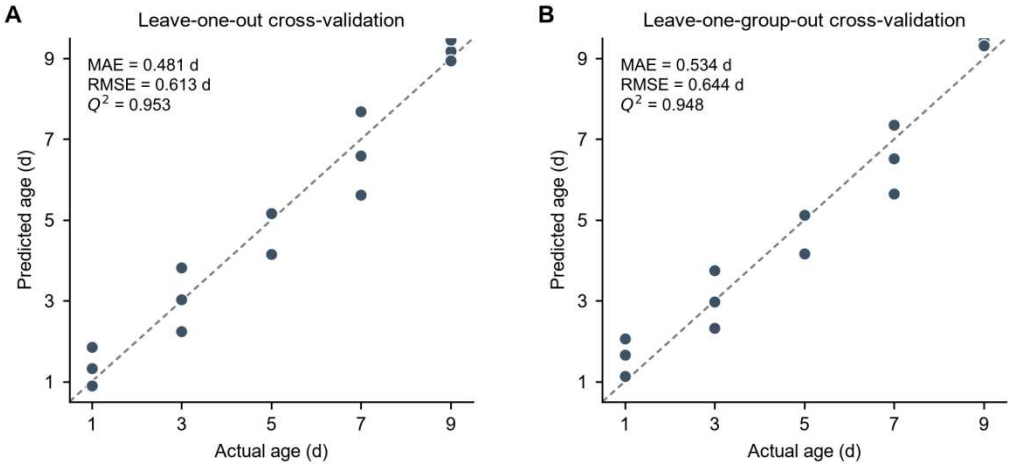

Fig. 7. Internal cross-validation of the two-marker model combining circRNA_1081 and TCONS_00010107 for post-emergence age estimation in *S. peregrina*. Predicted versus observed ages obtained by (A) leave-one-out cross-validation and (B) leave-one-group-out cross-validation, with sampling age as the grouping variable. Each point represents a prediction for a withheld biological sample. Dashed lines indicate perfect agreement between predicted and observed ages (y = x). Mean absolute error (MAE), root mean square error (RMSE), and the cross-validated coefficient of determination (Q^2) are shown. Age and prediction errors are expressed in days.

4.Discussion

Accurate determination of the developmental age of necrophagous insects is fundamental to estimating PMI_{min} from entomological evidence. Current molecular age-estimation studies have focused mainly on immature stages, including eggs, larvae, and pupae, whereas post-emergence adults remain comparatively underexplored[9, 41]. In *S. peregrina*, adults that have completed pupal development and emerged may still be present in environments associated with decomposing remains[42]. Estimating their post-emergence age could therefore provide additional temporal information beyond the immature stages. In this study, analysis of ovaries from adult female *S. peregrina* showed that the overall expression patterns of lncRNAs and circRNAs changed with age from D1 to D9, indicating that early post-emergence adults retain quantifiable molecular temporal information.

Notably, the numbers of differentially expressed ovarian lncRNAs and circRNAs in S. peregrina varied across successive post-emergence age comparisons, with the fewest detected in D7 vs D5 and an increase in D9 vs D7. This pattern suggests that the extent of detectable expression changes differed among age intervals and may be associated with changes in ovarian physiological state. Oocyte growth and follicular epithelial morphogenesis involve dynamic changes in cell shape and cytoskeletal organization[43, 44], while later chorion formation involves specialized follicle cell differentiation and secretion[45]. Against this background, the recurrent enrichment of actin filament organization among circRNA host genes in D3 vs D1, D5 vs D3, and D7 vs D5 may be associated with structural remodeling during the sampled post-emergence period. The enrichment of egg chorion assembly in D7 vs D5 is also compatible with maturation-related changes, although it does not establish the developmental stage of individual oocytes. Enrichment analyses of lncRNA cis-associated genes highlighted transcriptional regulation, development, and hormonal signaling, whereas those of circRNA host genes highlighted cytoskeletal organization, cell junctions, and signal transduction. These patterns provide a plausible biological context for the observed temporal expression changes. However, differences between the two analyses do not establish distinct functional roles for lncRNAs and circRNAs, and neither analysis demonstrates direct regulation of the enriched processes by the corresponding non-coding RNAs[46, 47]. Whole-ovary sampling introduces an additional consideration. Single-cell analyses in Drosophila have identified distinct transcriptional programs across ovarian cell types and developmental states [48]. By analogy, the age-associated expression changes observed here could reflect both changes within cells and shifts in the relative RNA contributions of different ovarian cell populations or follicle stages. These possibilities cannot be distinguished using the present bulk RNA data. Histological assessment or spatially resolved expression analysis would help identify the cellular sources of the candidate markers and clarify their relationship with ovarian maturation.

Wu et al. identified circRNAs with development-associated expression changes during intra-puparial development in *S. peregrina* and constructed an age-estimation model using qRT-PCR expression data and regression analysis[23]. Building on this work, the present study examined both lncRNAs and circRNAs in the ovaries of post-emergence adult females. Our findings support the potential of ovarian non-coding RNA expression profiles to provide age-related information during early adulthood. An important question, however, is whether these

markers primarily reflect chronological age, reproductive maturation, or a combination of both. In the related flesh fly *S. crassipalpis*, nutrient availability alters reproductive timing even after females have reached the minimum nutritional threshold for reproduction[49]. This finding raises the possibility that the relationship between ovarian expression and elapsed time may vary with physiological conditions. The present data establish an association with chronological age under the tested rearing conditions, but do not distinguish expression changes associated with elapsed time from those associated with reproductive maturation. Combining RNA measurements with ovarian morphological staging under contrasting nutritional conditions would help clarify the relative contributions of these processes.

Single-marker regression further showed that the age-related information captured by different non-coding RNAs was not identical. The eight single-marker models yielded LOOCV MAEs ranging from 0.767 to 1.740 d, with circRNA_0243, circRNA_1081, TCONS_00010107, and TCONS_00036632 showing relatively better performance. Based on these results, all pairwise combinations of the eight candidate RNAs were evaluated. The two-marker model combining circRNA_1081 and TCONS_00010107 achieved MAEs of 0.481 d and 0.534 d in LOOCV and LOGO-CV, respectively, with corresponding Q^2 values of 0.953 and 0.948. The similar performance obtained with the two validation strategies indicates that the model had good internal stability within the current dataset. Compared with single-RNA models, combining an lncRNA and a circRNA further reduced prediction error, suggesting that different classes of non-coding RNAs may provide partially complementary temporal information. However, this complementarity is currently supported mainly by the statistical prediction results, and its underlying molecular basis remains to be investigated.

From a forensic perspective, the model developed in this study estimates the post-emergence age of adult *S. peregrina* rather than PMI or PMI_{min} directly. Post-emergence adult age reflects only the time elapsed after completion of pupal development and therefore cannot be equated with the time since death[50]. However, when the association between the adult fly and the remains can be established, adult age may complement developmental information obtained from larvae, pupae, or empty puparia and help reconstruct a more complete entomological timeline. Its value lies primarily in extending the temporal range over which entomological evidence can be used, rather than replacing existing approaches for PMI_{min} estimation. This study also has several limitations.

First, the experiments were conducted under a single constant rearing condition and included only ovarian samples from female *S. peregrina* collected from D1 to D9. Temperature[51], nutrition[52], mating status, and reproductive status may all influence ovarian maturation and RNA expression, and the applicability of the present findings is therefore currently restricted to the conditions examined here. Second, qRT-PCR-based modeling included only 15 biological samples, and both two-marker selection and model performance assessment were based on the same dataset. The current predictive performance should therefore be regarded as an exploratory internal validation rather than a substitute for validation in an independent dataset. Future studies should include independent experimental batches and larger sample sizes and evaluate the stability of candidate RNAs and prediction models under different temperature, nutritional, and reproductive conditions. Reproducibility across geographic populations and other necrophagous fly species should also be assessed to define the practical applicability of these ovarian non-coding RNA markers. Overall, this study demonstrates clear age-related changes in ovarian lncRNAs and circRNAs after emergence in *S. peregrina* and supports their potential as molecular markers of adult age. These findings provide an experimental basis for extending molecular age estimation to post-emergence adults of necrophagous flies.

5.Conclusion

This study characterized ovarian lncRNA and circRNA expression in female *Sarcophaga peregrina* from D1 to D9 after emergence. Temporal expression analysis identified candidate age-associated non-coding RNAs, and qRT-PCR validated the age-related expression patterns of eight selected candidates. The two-marker model combining circRNA_1081 and TCONS_00010107 achieved mean absolute errors of 0.481 and 0.534 days under leave-one-out and leave-one-age-group-out cross-validation, respectively. These findings support ovarian lncRNAs and circRNAs as promising molecular markers of early adult age and extend molecular age estimation to post-emergence adults of necrophagous flies. When adult flies can be linked to the remains, their estimated post-emergence age may provide additional temporal information to support PMI estimation.

[1] G. Strete, A. Sălcudean, A.A. Cozma, C.C. Radu, Current Understanding and Future Research Direction for Estimating the Postmortem Interval: A Systematic Review, Diagnostics (Basel) 15(15) (2025).
[2] L. Franceschetti, A. Amadasi, V. Bugelli, G. Bolsi, M. Tsokos, Estimation of Late Postmortem Interval: Where Do We Stand? A Literature Review, Biology (Basel) 12(6) (2023).
[3] S. Matuszewski, Post-Mortem Interval Estimation Based on Insect Evidence: Current Challenges, Insects 12(4) (2021).
[4] G. Hu, L. Li, Y. Zhang, S. Shao, Y. Gao, R. Zhang, Y. Wang, Y. Zhang, Y. Guo, C. Kang, J. Wang, Y. Wang, A global perspective of forensic entomology case reports from 1935 to 2022, Int J Legal Med 137(5) (2023) 1535-1553.
[5] M.C. Lecheta, M.O. Moura, Estimating the Age of Forensically Useful Blowfly, Sarconesia chlorogaster (Diptera: Calliphoridae), Using Larval Length and Weight, J Med Entomol 56(4) (2019) 915-920.
[6] D. Martín-Vega, T.J. Simonsen, M.J.R. Hall, An effective method for preparing histological sections of blow fly intra-puparial stages for minimum PMI estimations, Int J Legal Med 138(5) (2024) 1947-1954.
[7] K. Hartmann, M. Bamberg, S. Seum, J. Amendt, M.A. Verhoff, R. Zehner, Establishment of a multiplex PCR-CE assay for the simultaneous and rapid analysis of age markers for Calliphora vicina pupae, Int J Legal Med 138(1) (2024) 187-196.
[8] Y. Shang, Y. Feng, L. Ren, X. Zhang, F. Yang, C. Zhang, Y. Guo, Pupal Age Estimation of Sarcophaga peregrina (Diptera: Sarcophagidae) at Different Constant Temperatures Utilizing ATR-FTIR Spectroscopy and Cuticular Hydrocarbons, Insects 14(2) (2023).
[9] J. Amendt, V. Bugelli, V. Bernhardt, Time Flies-Age Grading of Adult Flies for the Estimation of the Post-Mortem Interval, Diagnostics (Basel) 11(2) (2021).
[10] R. Estévez Dimitrov, J. Amendt, F. Rothweiler, R. Zehner, Age determination of the adult blow fly Lucilia sericata (Diptera: Calliphoridae) through quantitative pteridine fluorescence analysis, Forensic Sci Med Pathol 16(4) (2020) 641-648.
[11] K.E. Smith, R. Wall, E.J. Hayes, Measurement of age and population age structure in the blowfly, Lucilia sericata (Meigen) (Diptera: Calliphoridae), J Insect Physiol 44(10) (1998) 895-901.
[12] H.E. Moore, J.B. Butcher, C.R. Day, F.P. Drijfhout, Adult fly age estimations using cuticular hydrocarbons and Artificial Neural Networks in forensically important Calliphoridae species, Forensic Sci Int 280 (2017) 233-244.
[13] A.M. Tarone, K.C. Jennings, D.R. Foran, Aging blow fly eggs using gene expression: a feasibility study, J Forensic Sci 52(6) (2007) 1350-4.
[14] A.M. Tarone, D.R. Foran, Gene expression during blow fly development: improving the precision of age estimates in forensic entomology, J Forensic Sci 56 Suppl 1 (2011) S112-22.
[15] P. Boehme, P. Spahn, J. Amendt, R. Zehner, Differential gene expression during metamorphosis: a promising approach for age estimation of forensically important Calliphora vicina pupae (Diptera: Calliphoridae), Int J Legal Med 127(1) (2013) 243-9.
[16] Y. Shang, L. Ren, L. Yang, S. Wang, W. Chen, J. Dong, H. Ma, X. Qi, Y. Guo, Differential Gene Expression for Age Estimation of Forensically Important Sarcophaga peregrina (Diptera: Sarcophagidae) Intrapuparial, J Med Entomol 57(1) (2020) 65-77.

[17] C. Choudhary, S. Sharma, K.K. Meghwanshi, S. Patel, P. Mehta, N. Shukla, D.N. Do, S. Rajpurohit, P. Suravajhala, J.N. Shukla, Long Non-Coding RNAs in Insects, Animals (Basel) 11(4) (2021).
[18] Y. Shang, Y. Feng, L. Ren, X. Zhang, F. Yang, C. Zhang, Y. Guo, Genome-wide analysis of long noncoding RNAs and their association in regulating the metamorphosis of the Sarcophaga peregrina (Diptera: Sarcophagidae), PLoS Negl Trop Dis 17(6) (2023) e0011411.
[19] Y. Wang, Y. Fu, H. Cheng, C. Zhao, Q. Huang, M. Chang, W. Qiu, Y. Shen, D. Li, lncR26319/miR-2834/EndophilinA axis regulates oogenesis of the silkworm, Bombyx mori, Insect Sci 30(1) (2023) 65-80.
[20] J.O. Westholm, P. Miura, S. Olson, S. Shenker, B. Joseph, P. Sanfilippo, S.E. Celniker, B.R. Graveley, E.C. Lai, Genome-wide analysis of drosophila circular RNAs reveals their structural and sequence properties and age-dependent neural accumulation, Cell Rep 9(5) (2014) 1966-1980.
[21] M.M. Wiśniewska, M. Kolísko, P. Berková, M. Moos, H.O. Maaroufi, F.G. Noriega, M. Nouzova, Ovarian transcriptome analyses indicate that weak juvenile hormone signaling underlies the molecular basis of oogenesis deficiencies in mosquitoes, BMC Biol 23(1) (2025) 160.
[22] Y. Gao, L. Yang, Y. Chen, P. Liu, Y. Zhou, X. Chen, J. Gu, Aal-circRNA-407 regulates ovarian development of Aedes albopictus, a major arbovirus vector, via the miR-9a-5p/Foxl axis, PLoS Pathog 19(5) (2023) e1011374.
[23] H. Wu, H. Tang, X. Han, F.J. Ngando, Y. Shang, Y. Guo, Identification of circular RNAs as biomarkers for pupal age estimation and postmortem interval in forensically important Sarcophaga peregrina (Diptera: Sarcophagidae), Int J Legal Med 139(5) (2025) 2441-2455.
[24] C. Zhang, A.J. Kim, C. Rivera-Perez, F.G. Noriega, Y.J. Kim, The insect somatostatin pathway gates vitellogenesis progression during reproductive maturation and the post-mating response, Nat Commun 13(1) (2022) 969.
[25] D. Wei, R. Li, M.Y. Zhang, Y.W. Liu, Z. Zhang, G. Smagghe, J.J. Wang, Comparative Proteomic Profiling Reveals Molecular Characteristics Associated with Oogenesis and Oocyte Maturation during Ovarian Development of Bactrocera dorsalis (Hendel), Int J Mol Sci 18(7) (2017).
[26] L. Ren, Y. Shang, L. Yang, S. Wang, X. Wang, S. Chen, Z. Bao, D. An, F. Meng, J. Cai, Y. Guo, Chromosome-level de novo genome assembly of Sarcophaga peregrina provides insights into the evolutionary adaptation of flesh flies, Mol Ecol Resour 21(1) (2021) 251-262.
[27] D. Kim, J.M. Paggi, C. Park, C. Bennett, S.L. Salzberg, Graph-based genome alignment and genotyping with HISAT2 and HISAT-genotype, Nat Biotechnol 37(8) (2019) 907-915.
[28] M. Pertea, G.M. Pertea, C.M. Antonescu, T.C. Chang, J.T. Mendell, S.L. Salzberg, StringTie enables improved reconstruction of a transcriptome from RNA-seq reads, Nat Biotechnol 33(3) (2015) 290-5.
[29] S. Anders, P.T. Pyl, W. Huber, HTSeq--a Python framework to work with high-throughput sequencing data, Bioinformatics 31(2) (2015) 166-9.
[30] Y.J. Kang, D.C. Yang, L. Kong, M. Hou, Y.Q. Meng, L. Wei, G. Gao, CPC2: a fast and accurate coding potential calculator based on sequence intrinsic features, Nucleic Acids Res 45(W1) (2017) W12-w16.
[31] L. Sun, H. Luo, D. Bu, G. Zhao, K. Yu, C. Zhang, Y. Liu, R. Chen, Y. Zhao, Utilizing sequence intrinsic composition to classify protein-coding and long non-coding transcripts, Nucleic Acids Res 41(17) (2013) e166.
[32] A. Li, J. Zhang, Z. Zhou, PLEK: a tool for predicting long non-coding RNAs and messenger RNAs based on an improved k-mer scheme, BMC Bioinformatics 15(1) (2014) 311.

[33] R.D. Finn, A. Bateman, J. Clements, P. Coggill, R.Y. Eberhardt, S.R. Eddy, A. Heger, K. Hetherington, L. Holm, J. Mistry, E.L. Sonnhammer, J. Tate, M. Punta, Pfam: the protein families database, Nucleic Acids Res 42(Database issue) (2014) D222-30.
[34] B. Langmead, S.L. Salzberg, Fast gapped-read alignment with Bowtie 2, Nat Methods 9(4) (2012) 357-9.
[35] A. Roberts, L. Pachter, Streaming fragment assignment for real-time analysis of sequencing experiments, Nat Methods 10(1) (2013) 71-3.
[36] H. Li, R. Durbin, Fast and accurate short read alignment with Burrows-Wheeler transform, Bioinformatics 25(14) (2009) 1754-60.
[37] Y. Gao, J. Zhang, F. Zhao, Circular RNA identification based on multiple seed matching, Brief Bioinform 19(5) (2018) 803-810.
[38] M.I. Love, W. Huber, S. Anders, Moderated estimation of fold change and dispersion for RNA-seq data with DESeq2, Genome Biol 15(12) (2014) 550.
[39] L. Wang, Z. Feng, X. Wang, X. Wang, X. Zhang, DEGseq: an R package for identifying differentially expressed genes from RNA-seq data, Bioinformatics 26(1) (2010) 136-8.
[40] V. Wucher, F. Legeai, B. Hédan, G. Rizk, L. Lagoutte, T. Leeb, V. Jagannathan, E. Cadieu, A. David, H. Lohi, S. Cirera, M. Fredholm, N. Botherel, P.A.J. Leegwater, C. Le Béguec, H. Fieten, J. Johnson, J. Alföldi, C. André, K. Lindblad-Toh, C. Hitte, T. Derrien, FEELnc: a tool for long non-coding RNA annotation and its application to the dog transcriptome, Nucleic Acids Res 45(8) (2017) e57.
[41] S. Shao, L. Yang, G. Hu, L. Li, Y. Wang, L. Tao, Application of omics techniques in forensic entomology research, Acta Trop 246 (2023) 106985.
[42] M.J.R. Hall, The Relationship between Research and Casework in Forensic Entomology, Insects 12(2) (2021).
[43] S. Li, Z.Y. Liu, H. Li, S. Zhou, J. Liu, N. Sun, K.F. Yang, V. Dougados, T. Mangeat, K. Belguise, X.Q. Feng, Y. Liu, X. Wang, Basal actomyosin pulses expand epithelium coordinating cell flattening and tissue elongation, Nat Commun 15(1) (2024) 3000.
[44] C. Berg, M. Sieber, J. Sun, Finishing the egg, Genetics 226(1) (2024).
[45] A.D. Velentzas, P.D. Velentzas, N.E. Sagioglou, E.G. Konstantakou, A.K. Anagnostopoulos, M.M. Tsioka, V.E. Mpakou, Z. Kollia, C. Consoulas, L.H. Margaritis, I.S. Papassideri, G.T. Tsangaris, E. Sarantopoulou, A.C. Cefalas, D.J. Stravopodis, Targeted Downregulation of s36 Protein Unearths its Cardinal Role in Chorion Biogenesis and Architecture during Drosophila melanogaster Oogenesis, Sci Rep 6 (2016) 35511.
[46] F. Kopp, J.T. Mendell, Functional Classification and Experimental Dissection of Long Noncoding RNAs, Cell 172(3) (2018) 393-407.
[47] A.F. Nielsen, A. Bindereif, I. Bozzoni, M. Hanan, T.B. Hansen, M. Irimia, S. Kadener, L.S. Kristensen, I. Legnini, M. Morlando, M.T. Jarlstad Olesen, R.J. Pasterkamp, S. Preibisch, N. Rajewsky, C. Suenkel, J. Kjems, Best practice standards for circular RNA research, Nat Methods 19(10) (2022) 1208-1220.
[48] A. Jevitt, D. Chatterjee, G. Xie, X.F. Wang, T. Otwell, Y.C. Huang, W.M. Deng, A single-cell atlas of adult Drosophila ovary identifies transcriptional programs and somatic cell lineage regulating oogenesis, PLoS Biol 18(4) (2020) e3000538.
[49] F.J. Wessels, R. Kristal, F. Netter, J.D. Hatle, D.A. Hahn, Does it pay to delay? Flesh flies show adaptive plasticity in reproductive timing, Oecologia 165(2) (2011) 311-20.

[50] V. Bernhardt, W. Pogoda, M.A. Verhoff, S.W. Toennes, J. Amendt, Estimating the age of the adult stages of the blow flies Lucilia sericata and Calliphora vicina (Diptera: Calliphoridae) by means of the cuticular hydrocarbon n-pentacosane, Sci Justice 57(5) (2017) 361-365.
[51] A.C.P. Gandara, D. Drummond-Barbosa, Warm and cold temperatures have distinct germline stem cell lineage effects during Drosophila oogenesis, Development 149(5) (2022).
[52] M.F. Camus, A. Chakraborty, M. Reuter, Disentangling the reproductive and metabolic transcriptional responses to diet in Drosophila melanogaster, G3 (Bethesda) 16(4) (2026).

Supplementary Files

This is a list of supplementary files associated with this preprint. Click to download.

- supplementary.zip